Analysis of the Radiation Properties of a Point Source on a Uniaxially Anisotropic Meta−Substrate and the Application to a High−Efficiency Antenna

Attieh Shahvarpour [#1], Alejandro Alvarez Melcón [*2], Christophe Caloz [#3]

[#]*Electrical Engineering Department, École Polytechnique de Montréal*
Poly-Grames Research Center, Pavillon Lassonde, 2500, Chemin Polytechnique
Montréal, QC, H3T 1J4, Canada
[1]attieh.shahvarpour@polymtl.ca
[3]christophe.caloz@polymtl.ca

[*]*Electrical Engineering Department, Technical University of Cartagena*
Campus Muralla del Mar-Antiguones, 30202 Cartagena (Murcia), Spain
[2]alejandro.alvarez@upct.es

***Abstract*— The radiation efficiency of a point electric source on a loss-less uniaxially anisotropic meta-substrate is computed by the mixed potential integral equation technique. For this purpose, the multilayered Green's functions of the structure are derived from the spectral domain transmission line model of the medium. The efficiency of the antenna is compared for different permittivities and permeabilities of the meta-substrate with fixed TE and TM wave numbers. It is shown that at certain frequencies the radiation efficiency is enhanced as the ratio of the permeability over permittivity is increased. This suggests that an antenna on a mushroom type meta-substrate or a meta-substrate which is constructed from the stacked split ring resonators (SRR) in the plane of the substrate may exhibit a high radiation efficiency close to the resonant frequencies of the metallic loops, as compared to a conventional substrate.**

I. Introduction

Recently, meta-substrates, which are planar artificial dielectrics with unusual properties, have been studied and proposed for several applications such as bandwidth enhancement of patch antennas [1], [2], backfire-to-endfire leaky-wave antennas [3], microwave systems miniaturization [4] and analog signal processing [5]. These applications are made possible by engineering the permeability and permittivity of the meta-substrates. However, in most of these studies the meta-substrates have been modeled as simplified isotropic media whereas they are actually strongly anisotropic materials.

In this paper, meta-substrates with uniaxially anisotropic permittivity and permeability are analyzed and their effects on the efficiency enhancement of a radiating point electric source on top of them are studied. Two meta-substrate configurations are considered. The first structure is a mushroom type configuration constructed from vias along the perpendicular axis to the substrate interface and the metallic loops between the adjacent vias [3], [6]. The second type is a meta-substrate that includes an array of stacked split ring resonators (SRRs) in the plane of the substrate.

For the analysis, a multilayered Green's function approach [7] is used to compute the space and surface modes' Green's functions. The free-space and meta-substrate far-fields are obtained from the asymptotic approximations [8]-[10]. Finally, the efficiency of the antenna is calculated from the space wave power and the power in the meta-substrates carried by the surface modes.

II. Uniaxially Anisotropic Meta-substrates

Fig. 1a shows the mushroom type meta-substrates with the vias along the z axis and the metallic loops between the adjacent vias in the xz and yz planes. Fig. 1b shows the stacked SRR meta-substrate with the SRRs in the xy plane of the host medium. The short vias along the z axis produce a Drude permittivity [11] along this axis, while the permittivity along the other axes is that of the host medium. The permeability along the axis perpendicular to the metallic loops exhibits a Lorentz behavior [12] whereas the permeability along the other axes is that of the host medium. Thus, according to Fig. 1c, both meta-substrate structures show an effective anisotropic behavior with the following effective permittivity and permeability tensors

$$\bar{\bar{\varepsilon}} = \begin{pmatrix} \varepsilon_\rho & 0 & 0 \\ 0 & \varepsilon_\rho & 0 \\ 0 & 0 & \varepsilon_z \end{pmatrix}, \quad \bar{\bar{\mu}} = \begin{pmatrix} \mu_\rho & 0 & 0 \\ 0 & \mu_\rho & 0 \\ 0 & 0 & \mu_z \end{pmatrix}. \qquad (1)$$

III. Spectral Domain Transmission Line Model and Green's Functions of the Uniaxially Anisotropic Meta-substrate

The multilayered Green's functions are computed from the transmission line model of each layer. Assuming the time dependence $\exp(+j\omega t)$, the spectral domain transmission line equations have the form [8]

$$\frac{d\tilde{I}^i}{dz} = -jY^i k_z^i \tilde{V}^i + \tilde{I}_g, \ \frac{d\tilde{V}^i}{dz} = -jZ^i k_z^i \tilde{I}^i, \qquad (2)$$

where $\tilde{V}^i$, $\tilde{I}^i$, Z^i, Y^i , $\tilde{I}_g$ and k_z^i are the spectral-domain voltage and current, impedance, admittance, current source

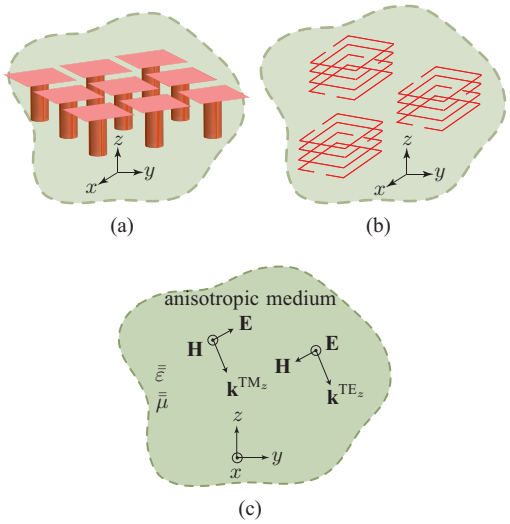

Fig. 1: Various uniaxially anisotropic meta-substrate structures. (a) Mushroom type. (b) Stacked split ring resonator (SRR) type. (c) Effective medium.

and the wave number along the z axis of the transmission line, respectively, for $i \equiv \mathrm{TM}_z/\mathrm{TE}_z$ modes. In addition $Z_c^i = \sqrt{Z^i/Y^i}$ and $\beta^i = \sqrt{Z^i Y^i}k_z^i$ are the characteristic impedance and the propagation constant of the transmission line, respectively. The transmission line models of the TM_z and TE_z modes, with the same form as Eqs. (2), are next determined by inserting the tensors of Eqs. (1) into Maxwell's equations,

$$\nabla \times \mathbf{H} = j\omega\bar{\bar{\varepsilon}}\mathbf{E} + \mathbf{J}, \tag{3a}$$

$$\nabla \times \mathbf{E} = -j\omega\bar{\bar{\mu}}\mathbf{H}. \tag{3b}$$

A. TM_z Modes

Inserting Eqs. (1) into Eqs. (3) for the TM_z modes ($H_z = 0$) and writing the resulting equations in the spectral domain, where $\partial/\partial x \to jk_x^{TM_z}$ and $\partial/\partial y \to jk_y^{TM_z}$, and assuming a horizontal electric point source $\tilde{\mathbf{J}} = 1/2\pi\delta(z-z')\mathbf{a}_x$, yields the TM_z transmission line equations in the form of Eq. (2) as follows

$$\frac{d}{dz}\left[\frac{-\omega\varepsilon_z}{k_x^{TM_z}}\tilde{G}_{EJ}^{zx,TM_z}\right] = -j\left(\frac{\omega\varepsilon_\rho}{k_z^{TM_z}}\right)k_z^{TM_z}\left[\frac{-{k_\rho}^2}{{k_x^{TM_z}}^2}\tilde{G}_{EJ}^{xx,TM_z}\right] + \tilde{J}_x, \tag{4a}$$

$$\frac{d}{dz}\left[\frac{-{k_\rho^{TM_z}}^2}{{k_x^{TM_z}}^2}\tilde{G}_{EJ}^{xx,TM_z}\right] = -j\left(\frac{k_z^{TM_z}}{\omega\varepsilon_z}\right)k_z\left[\frac{-\omega\varepsilon_z}{k_x^{TM_z}}\tilde{G}_{EJ}^{zx,TM_z}\right], \tag{4b}$$

where $\tilde{G}_{EJ}^{xx,TM_z}$ and $\tilde{G}_{EJ}^{zx,TM_z}$ are the spectral domain electric field Green's functions along the x and z axes, respectively, produced by the electric source along the x axis, $k_z^{TM_z}$ is the longitudinal wave number, ${k_\rho^{TM_z}}^2 = {k_x^{TM_z}}^2 + {k_y^{TM_z}}^2$ is the square of the transverse wave number and ${k_\rho^{TM_z}}^2 + {k_z^{TM_z}}^2 = \omega^2\mu_\rho\varepsilon_z = {k^{TM_z}}^2$, where k^{TM_z} is the TM_z wave number. The analogy of the equivalent transmission line model of Eqs. (4) with Eqs. (2) results in

$$\tilde{G}_{EJ}^{xx,TM_z} = \frac{-{k_x^{TM_z}}^2}{{k_\rho^{TM_z}}^2}\tilde{V}^{TM_z},\ \tilde{G}_{EJ}^{zx,TM_z} = \frac{-k_x^{TM_z}}{\omega\varepsilon_z}\tilde{I}^{TM_z}, \tag{5}$$

and $Z_c^{TM_z} = k_z^{TM_z}/(\omega\varepsilon_\rho)\sqrt{\varepsilon_\rho/\varepsilon_z}$ and $\beta^{TM_z} = \sqrt{\varepsilon_\rho/\varepsilon_z}k_z^{TM_z}$. Next, the magnetic Green's functions are computed from substituting Eqs. (5) into spectral domain Maxwell's equations as follows

$$\tilde{G}_{HJ}^{xx,TM_z} = \frac{k_x^{TM_z}k_y^{TM_z}}{{k_\rho^{TM_z}}^2}\tilde{I}^{TM_z},\ \tilde{G}_{HJ}^{zx,TM_z} = 0. \tag{6}$$

B. TE_z Modes

The TE_z ($E_z = 0$) transmission line model is obtained by an approach dual to that used in Sec. III-A for the TM_z parameters. The resulting equations are

$$\frac{d}{dz}\left[\frac{-{k_\rho^{TE_z}}^2}{k_x^{TE_z}k_y^{TE_z}}\tilde{G}_{HJ}^{xx,TE_z}\right] = -j\left(\frac{k_z^{TE_z}}{\omega\mu_z}\right)k_z^{TE_z}\left[\frac{-\omega\mu_z}{k_y^{TE_z}}\tilde{G}_{HJ}^{zx,TE_z}\right] + \tilde{J}_x, \tag{7a}$$

$$\frac{d}{dz}\left[\frac{-\omega\mu_z}{k_y^{TE_z}}\tilde{G}_{HJ}^{zx,TE_z}\right] = -j\left(\frac{\omega\mu_\rho}{k_z^{TE_z}}\right)k_z^{TE_z}\left[\frac{-{k_\rho^{TE_z}}^2}{k_x^{TE_z}k_y^{TE_z}}\tilde{G}_{HJ}^{xx,TE_z}\right], \tag{7b}$$

where $\tilde{G}_{HJ}^{xx,TE_z}$ and $\tilde{G}_{HJ}^{zx,TE_z}$ are the spectral domain magnetic field Green's functions along the x and z axes, respectively, produced by the electric source along the x axis, $k_z^{TE_z}$ is the longitudinal wave number, ${k_\rho^{TE_z}}^2 = {k_x^{TE_z}}^2 + {k_y^{TE_z}}^2$ is the square of the transverse wave number and ${k_\rho^{TE_z}}^2 + {k_z^{TE_z}}^2 = \omega^2\mu_z\varepsilon_\rho = {k^{TE_z}}^2$, where k^{TE_z} is the TE_z wave number. The analogy of the equivalent transmission line model of Eqs. (7) and Eqs. (2) leads to

$$\tilde{G}_{HJ}^{xx,TE_z} = -\frac{k_x^{TE_z}k_y^{TE_z}}{{k_\rho^{TE_z}}^2}\tilde{I}^{TE_z},\ \tilde{G}_{HJ}^{zx,TE_z} = -\frac{k_y^{TE_z}}{\omega\mu_z}\tilde{V}^{TE_z}, \tag{8}$$

and $Z_c^{TE_z} = \omega\mu_z/k_z^{TE_z}\sqrt{\mu_\rho/\mu_z}$ and $\beta^{TE_z} = \sqrt{\mu_\rho/\mu_z}k_z^{TE_z}$. The electric Green's functions are computed by substituting Eqs. (8) into spectral domain Maxwell's equations as follows

$$\tilde{G}_{EJ}^{xx,TE_z} = -\frac{{k_y^{TE_z}}^2}{{k_\rho^{TE_z}}^2}\tilde{V}^{TE_z},\ \tilde{G}_{EJ}^{zx,TE_z} = 0. \tag{9}$$

C. Vector Potentials Green's Functions

In the mixed potential integral equations with Sommerfeld choice for the potentials [7] with a source along x, it is assumed that the electric vector potential Green's function $\bar{\bar{\mathbf{G}}}_F = 0$, while the magnetic vector potential Green's functions $\bar{\bar{\mathbf{G}}}_A = \left(\mathbf{a}_x G_A^{xx} + \mathbf{a}_z G_A^{zx}\right)\mathbf{a}_x$, where G_A^{xx} and G_A^{zx} are the

vector potential Green's function produced by $\tilde{J}_x$ along the x and z axes, respectively and we have [13]

$$\bar{\bar{\mathbf{G}}}_{HJ} = \bar{\bar{\mu}}^{-1} \nabla \times \bar{\bar{\mathbf{G}}}_A, \tag{10}$$

where $\bar{\bar{\mathbf{G}}}_{HJ} = \bar{\bar{\mathbf{G}}}_{HJ}^{TM_z} + \bar{\bar{\mathbf{G}}}_{HJ}^{TE_z}$ is the total magnetic Green's functions with $\bar{\bar{\mathbf{G}}}_{HJ}^{TM_z}$ and $\bar{\bar{\mathbf{G}}}_{HJ}^{TE_z}$ obtained from Eqs. (6) and (8), respectively, with $k_{\rho,x,y}^{TM_z} = k_{\rho,x,y}^{TE_z} = k_{\rho,x,y}$. Substituting $\bar{\bar{\mu}}$ from Eq. (1) into Eqs. (10) and then substituting $\tilde{\mathbf{G}}_{HJ}^{xx,TM_z}$ and $\tilde{\mathbf{G}}_{HJ}^{zx,TM_z}$ from Eqs. (6) and $\tilde{\mathbf{G}}_{HJ}^{xx,TE_z}$ and $\tilde{\mathbf{G}}_{HJ}^{zx,TE_z}$ from (8) into the resulting equation leads to

$$\tilde{\mathbf{G}}_A^{xx} = \frac{1}{j\omega} V^{TE_z}, \tag{11a}$$

$$\tilde{\mathbf{G}}_A^{zx} = \frac{\mu_\rho}{jk_y} \left(\frac{k_x k_y}{k_\rho^2} I^{TM_z} - \frac{k_x k_y}{k_\rho^2} I^{TE_z} \right). \tag{11b}$$

IV. Radiation Properties Analysis

A. Radiation Pattern

The spectral and spatial domain Green's functions are related through the double Fourier transformation as follows

$$G_A(x,y,z) = \frac{1}{2\pi} \int_{-\infty}^{+\infty} \int_{-\infty}^{+\infty} \tilde{G}_A(k_x k_y, z) e^{jk_x x} e^{jk_y y}\, dk_x\, dk_y. \tag{12}$$

Assuming that the radiating spectral domain Green's function dependence on the z axis is that of a pure spherical wave traveling in the upper semi-infinite free-space, $\tilde{G}_A(k_x, k_y, z) = \tilde{g}_A(k_x, k_y) \exp(-jk_{z0}z)$, where k_{z0} is the propagation constant along z in the free space. Applying the far-field asymptotic approximations ($k_\rho \rho, k_0 r \to \infty$) [8], [9], the far-field Green's function associated with the space waves is obtained as follows

$$G_A(x,y,z) = jk_0 \cos\theta \tilde{g}_A(k_x, k_y) \frac{\exp(-jk_0 r)}{r}, \tag{13}$$

where k_0 is the free-space wave number. Next, the electric field and thus the radiation pattern is computed from

$$\mathbf{E}(x,y,z) = -j\omega \overline{\overline{\mathbf{G}}}_A(x,y,z).\mathbf{a}_x. \tag{14}$$

B. Radiation Efficiency

For a lossless antenna, the radiation efficiency η is [14]

$$\eta = \frac{P_{rad}}{P_{rad} + P_{sw}}, \tag{15}$$

where P_{rad} and P_{sw} are the radiation and the surface modes powers, respectively.

1) Radiation Power: P_{rad} is calculated as follows

$$P_{rad} = \int_0^{2\pi} \int_0^{\pi/2} \mathbf{S}_{r,av}.\mathbf{a}_r r^2 \sin\theta\, d\theta\, d\phi \tag{16}$$

where $\mathbf{S}_{r,av} = \frac{1}{2}\mathrm{Re}[\mathbf{E} \times \mathbf{H}^*]$ is the Poynting vector with the fields given by Eq. (14). This power includes both the space-wave and leaky-wave radiation powers.

2) Surface Modes' Power: P_{sw} is calculated considering cylindrical wave associated to a surface mode as follows

$$P_{sw} = \int_0^{2\pi} \int_0^{d} \mathbf{S}_{sw,av}.\mathbf{a}_\rho \rho\, dz\, d\phi, \tag{17}$$

where $\mathbf{S}_{sw,av}$ is the far-field ($k_\rho \rho \to \infty$) Poynting vector inside the meta-substrate. In a lossless dielectric, the far-field Sommerfeld transformations are computed from the residues of the spectral Green's functions as follows [10]

$$G_A(\rho) = -\pi j \sum_i H_n^{(2)}(k_{\rho_i}\rho) k_{\rho_i}^{n+1} R_i, \tag{18}$$

where $n = 0$ for the zeroth order Sommerfeld transformation and R_i is the residue of $\tilde{G}_A$ at the poles k_{ρ_i}. As a result, in the meta-substrate

$$E_\phi = (-j\omega)\pi j \sin\phi \sum_i H_0^{(2)}(k_{\rho_i}\rho) k_{\rho_i} R_i^{xx}, \tag{19a}$$

$$E_z = (j\omega)\pi j \sum_i H_0^{(2)}(k_{\rho_i}\rho) k_{\rho_i} R_i^{zx}. \tag{19b}$$

By inserting $\bar{\mu}$ from Eq. (1) into Maxwell's equations (Eq. 3b), and then applying the far-field approximations ($E_\rho = 0$ and $H_\rho = 0$), the magnetic fields are obtained from the electric fields (Eqs. (19)) as follows

$$H_\phi = \frac{1}{j\omega\mu_\rho} \left[(-j\omega)\pi j \sum_i H_1^{(2)}(k_{\rho_i}\rho) k_{\rho_i}^2 R_i^{zx} \right], \tag{20a}$$

$$H_z = \frac{1}{j\omega\mu_z} \sin\phi \left[(-j\omega)\pi j \sum_i H_1^{(2)}(k_{\rho_i}\rho) k_{\rho_i}^2 R_i^{xx} \right]. \tag{20b}$$

The surface modes' Poynting vector and therefore the average power are computed by substituting Eqs. (19) and (20) into Eq. (17) and by using the far-field asymptotic ($k_\rho \rho \to \infty$) expression of the Hankel functions $H_p^{(2)}(k_\rho \rho) = \sqrt{2/(\pi k_\rho \rho)} \exp\left[-j\left(k_\rho \rho - p\pi/2 - \pi/4\right)\right]$ [13].

C. Results and Discussion

Now we will compute the efficiency of the uniaxial meta-substrate with thickness $d = 3$ mm at $f = 17$ GHz for different permeabilities and permittivities. In order to compare the radiation efficiency of the point source on substrates with identical electrical dimensions, the permittivities and permeabilities of the meta-substrate are chosen so that $\mu_\rho \varepsilon_z$ and $\mu_z \varepsilon_\rho$ are constant, since the electrical dimensions of the meta-substrate are related to ${k^{TM_z}}^2/\omega^2 = \mu_\rho \varepsilon_z$ and ${k^{TE_z}}^2/\omega^2 = \mu_z \varepsilon_\rho$ for the TM_z and TE_z modes, respectively.

In this study, we set $\mu_\rho \varepsilon_z = 5\mu_0\varepsilon_0$ and $\mu_z \varepsilon_\rho = 5\mu_0\varepsilon_0$. The properties of the slab are chosen so that the conventional isotropic substrate operates above the TM_z and TE_z surface mode cutoff frequencies, in order to permit the observation of the effect of the both TM and TE modes. The efficiencies for the 4 cases are shown in Tab. I. As shown in the table, the isotropic conventional substrate (case 1) has the lowest

TABLE I

COMPARISON OF THE RADIATION EFFICIENCY OF A HORIZONTAL POINT SOURCE ON A CONVENTIONAL SUBSTRATE AND META-SUBSTRATES WITH DIFFERENT PERMITTIVITIES AND PERMEABILITIES COMPUTED BY (15) ($d = 3$ mm, $f = 17$ GHz, $\mu_\rho \varepsilon_z = 5\mu_0\varepsilon_0$ and $\mu_z \varepsilon_\rho = 5\mu_0\varepsilon_0$)

case	μ_ρ/μ_0	$\varepsilon_z/\varepsilon_0$	μ_z/μ_0	$\varepsilon_\rho/\varepsilon_0$	efficiency η	surface modes
1 (conventional isotropic substrate)	1	5	1	5	%7.03	TM_0 and TE_1
2 (anisotropic meta-substrate)	$2\sqrt{5}$	$\sqrt{5}/2$	1	5	%38.52	TM_0, TE_1 and TM_1
3 (isotropic magnetic meta-substrate)	$2\sqrt{5}$	$\sqrt{5}/2$	$2\sqrt{5}$	$\sqrt{5}/2$	% 35.08	TM_0 and TE_1
4 (anisotropic meta-substrate)	1	5	$2\sqrt{5}$	$\sqrt{5}/2$	%29.25	TM_0

efficiency while the anisotropic meta-substrate with the high μ_ρ/ε_z (case 2) exhibits the highest efficiency. The isotropic magnetic meta-substrate (case 3) has a higher efficiency than the conventional isotropic substrate (case 1). Although the number of surface modes in the anisotropic meta-substrate of the case 2 is larger than in the other cases, the energy coupled to the space modes is larger, thus resulting in a higher radiation efficiency.

In summary, at $f = 17$ GHz the efficiency of the structure is proportional to μ_ρ/ε_z and μ_z/ε_ρ. Moreover, comparing the cases 2 and 4 with $(\mu_z/\varepsilon_\rho)_{\text{case 2, 4}} = (\mu_\rho/\varepsilon_z)_{\text{case 4, 2}}$, shows that at this frequency the effect of increasing μ_ρ/ε_z in the efficiency enhancement is more significant. The results suggest that the mushroom type (Fig. 1a) and the stacked SRR meta-substrates (Fig. 1b), corresponding to the cases 2 and 4, respectively, may provide a high efficiency antenna close to the resonant frequencies of their metallic loops, as compared to the conventional substrate (case 1).

Fig. 2 shows the radiation patterns of the 4 cases shown in Tab. I. As demonstrated in this figure, the radiation pattern for the isotropic conventional substrate and the isotropic magnetic meta-substrate (cases 1 and 3, respectively) are similar. However, the radiation pattern of the case 4 is more directive than the other cases.

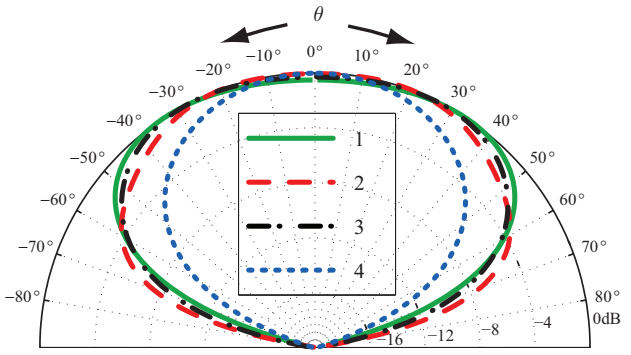

Fig. 2: Comparison of the radiation patterns of the 4 cases in Tab. I (E_{tot} at $\phi = 45°$).

V. CONCLUSIONS

The radiation efficiency of a point electric source on a lossless uniaxially anisotropic meta-substrate was calculated by the mixed potential integral equations with the Sommerfeld transformation. The multilayered Green's functions of the structure were computed from the spectral domain transmission line model of the medium. The efficiency of the antenna was compared for the different meta-substrate permittivities and permeabilities. The highest efficiency was obtained for the case of the highest ratio of permeability over permittivity. This suggests that at certain frequencies the antenna on the mushroom type or the stacked split ring resonators meta-substrates may exhibit a high radiation efficiency close to the resonant frequencies of the metallic loops, as compared to the conventional substrates.

ACKNOWLEDGEMENT

This work has been supported by projects TEC2007-67630-C03-02 of Spanish MEC and 08833/PI/08 of Fundacion Seneca.

REFERENCES

[1] P. M. T. Ikonen, K. N. Rozanov, A. V. Osipov, P. Alitalo, and S. A. Tretyakov, "Magnetodielectric substrates in antenna miniaturization: potentials and limitations," *IEEE Trans. Antennas Propagat.*, vol. 54, no. 11, pp. 3391-3399, Nov. 2006.

[2] H. Mosallaei and K. Sarabandi, "Design and modeling of patch antenna printed on magneto-dielectric embedded-circuit metasubstrate," *IEEE Trans. Antennas Propagat.*, vol. 55, no. 1, pp. 45-52, Jan. 2007.

[3] H. V. Nguyen and C. Caloz, "Anisotropic backward-wave meta-susbtrate and its application to a microstrip leaky-wave antenna," in *Proc. CNC/USNC URSI National Radio Science Meeting*, Ottawa, ON, Canada, July 2007.

[4] M. Coulombe, H. V. Nguyen, and C. Caloz, "Substrate integrated artificial dielectric (SIAD) structure for miniaturized microstrip circuits," *IEEE Antennas and Wireless Propagat. Lett.*, vol. 6, no. 6, pp. 575-579, Dec. 2007.

[5] M. Coulombe and C. Caloz, "Reflection-type artificial dielectric substrate microstrip dispersive delay line (DDL) for analog signal processing," *IEEE Trans. Microwave Theory Tech.*, vol. 57, no. 7, pp. 1714-1723, July 2009.

[6] D. Sievenpiper, L. Zhang, R. F. J. Broas, N. G. Alexopolous, and E. Yablonovitch, "High-impedance electromagnetic surfaces with a forbidden frequency band," *IEEE Trans. Microwave Theory Tech.*, vol. 47, no. 11, pp. 2059-2074, Nov. 1999.

[7] J. R. Mosig, "Integral equation techniques," in *Numerical Techniques for Microwave and Millimeter-wave Passive Structures*, T. Itoh, Ed., Wiley InterSci., ch. 3, pp. 133-213, NY, 1989.

[8] L. B. Felsen and N. Marcuvitz, *Radiation and scattering of Waves*, Prentice-Hall/IEEE Press, NY, 1996.

[9] J. R. Mosig, and F. E. Gardiol, chap. 3 in P. W. Hawkes (editor), *Advances in Electronics and Electron Physics*, Academic Press, NY, vol. 59, 1982.

[10] J. R. Mosig and A. A. Melcon, "Green's functions in lossy layered media: integration along the imaginary axis and asymptotic behavior," *IEEE Trans. Antennas Propagat.*, vol. 51, no. 12, pp. 3200-3208, Dec. 2003.

[11] S. A. Tretyakov, *Analytical Modeling in Applied Electromagnetics*, Artech House, Norwood, MA, 2003.

[12] J. B. Pendry, A. J. Holden, D. J. Robbins, and W. J. Stewart, "Magnetism from conductors and enhanced non-linear phenomena," *IEEE Trans. Microwave Theory Tech.*, vol. 47, no. 11, pp. 2075-2084, Nov. 1999.

[13] C. A. Balanis, *Advanced Engineering Electromagnetics*, John-Wiley, Inc., NY, 1989.

[14] D. R. Jackson and N. G. Alexopoulos, "Simple approximate formulas for input resistance, bandwidth, and efficiency of a resonant rectangular patch," *IEEE Trans. Antennas Propagat.*, vol. 39, no. 3, pp. 407-410, March 1991.